

Importance of Correlations for Neural Quantum States

Fabian Döschl^{1,2,*} and Annabelle Bohrdt^{1,2}

¹*Ludwig-Maximilians-University Munich, Theresienstr. 37, Munich D-80333, Germany*

²*Munich Center for Quantum Science and Technology, Schellingstr. 4, Munich D-80799, Germany*

(Dated: August 21, 2025)

Neural quantum states (NQS) have emerged as a powerful variational ansatz for representing quantum many-body wave functions. Their internal mechanisms, however, remain poorly understood. We investigate the role of correlations for NQS-like quantum state representation by employing a correlation-based interpretable neural network architecture and thereafter proving our observations based on Boolean function theory. The correlator neural network demonstrates that, even for simple product states, up to all system-size correlation orders in the chosen computational basis are required to represent a quantum state faithfully. We explain these observations using the Fourier expansion, which reveals the correlator basis as the effective basis of the internal NQS structure, the resulting necessity for high-order correlations, potential linear dependencies in constrained Hilbert spaces, and connections between spin basis-rotations and the correlator basis. Furthermore, we analyze how activation functions, network architectures, and choice of reference basis influence correlation requirements. Our results provide new insights and a better understanding of the internal structure and requirements of NQS, enabling a more systematic use of NQS in future research.

I. INTRODUCTION

Two-dimensional quantum systems pose one of the most interesting challenges for current quantum many-body physics, as they are central to our understanding of high-temperature superconductivity, effects in strongly correlated spin systems, and topological phases. However, studying these systems with analytical or numerical methods is notoriously difficult.

State-of-the-art methods, such as tensor network methods (TN) or quantum Monte Carlo (QMC) approaches are limited in their capability to find and represent quantum states in two-dimensional systems [1–4]. Recently, Carleo and Troyer proposed a variational ansatz that uses the expressive power of neural networks to represent quantum states [5]. These so called neural quantum states (NQS) have shown remarkably good performance for many quantum systems [6–10] and have proven capable of capturing quantum states with sign problem (limitation of QMC) [11–15] or volume law entanglement (limitation of TN) [16–18]. However, unlike TN and QMC, NQS operate as a black-box method, making their controllability and a general understanding of how they work and when they fail still elusive. In particular, it is unclear how the network’s internal structure is related to the correlations in the target quantum state.

Since the introduction of neural quantum states, there has been a significant interest in understanding their representational power [16, 17, 19], optimization properties [6, 20–24], and practical limitations [25]. Despite the difficulty in analyzing and interpreting these non-linear variational functions, several studies have investigated the properties of neural quantum states analytically. A central result, extending beyond the study of NQS, is

the proof that neural networks, given a potentially exponential number of parameters, can approximate any continuous function [26–28]. Although this universality also applies to the NQS-like representation of arbitrary quantum state wave functions, it does not guarantee parameter efficiency. Nevertheless, in practice, we know from many numerical [29–34] and analytical [16, 19, 35–38] examples that there exists, in many cases, an efficient representation of physically relevant quantum states.

However, despite knowing about the promising properties of neural quantum states, it is often extremely challenging to fine-tune a network architecture for a specific quantum system such that we obtain the best results. A major hurdle for the optimization of NQS architectures is the fact that we often lack a clear understanding of the internal mechanisms of neural networks.

A possibility to achieve a better understanding of the working principle is to draw connections between the neural network and the underlying correlations in the system. A step in this direction was taken in the article [39], where weighted correlations (dominant terms in the Hamiltonian) were added to a restricted Boltzmann machine to improve convergence.

However, instead of improving a certain network architecture, we aim to reveal the required internal network structure for simulating quantum states. From the machine learning perspective, this was already done for phase and image classification tasks, where correlation based neural networks have been used to determine the important physical features for a successful characterization in terms of higher-order correlations [40–43]. The crucial idea for these interpretable neural network architectures is to replace the standard non-linear activation function by a controlled expansion in higher-order correlations of the input, e.g. spin-spin correlations. Through regularization path analysis or tuning the maximal order of correlations considered as a hyperparameter, it is then possible to determine the most relevant correlation

* Fa.Doeschl@physik.uni-muenchen.de

orders for a given *classification* task.

In these cases, it was enough to use low correlation orders (up to fourth order) to distinguish different phases. Yet, these insights do not directly transfer to quantum states, raising the question of which correlations are important to represent a quantum state, rather than merely characterizing it. Since representation requires the full set of wave function coefficients, it may depend on correlations far beyond those relevant for phase detection.

In this paper, we address the question of which correlations are essential to represent a quantum state systematically. Using the real valued correlator transformer architecture [42], we can control accessible correlation orders of the NQS and study their impact on the representational power for two paradigmatic models: the two dimensional Ising model and the toric code model. In combination with analytical methods, we identify conditions under which high correlation orders are unavoidable, even for simple product states. This stems from the fact that the effective internal basis that the NQS uses to represent a quantum state, i.e. in which the connection between neural network parameters and wave function coefficient arises naturally, is not the reference spin (or Fock) basis, but the correlator basis. Our analysis allows to draw conclusions about the desired NQS structure, enabling a structured optimization of its activation functions and architectures.

II. NEURAL QUANTUM STATES

For an exact representation of a quantum state, one generally needs Hilbert space dimension H_{dim} many wave function coefficients to describe the system in terms of basis states,

$$|\Psi_\lambda\rangle = \sum_{\sigma} \psi_{\text{state}}^{\sigma} |\sigma\rangle. \quad (1)$$

Without loss of generality, we will mainly focus on spin-1/2 systems in this paper. As storing and evaluating all H_{dim} coefficients is exponentially costly, one searches for a function that efficiently approximates these wave function coefficients $\psi_{\text{state}} = \{\psi_{\text{state}}^{\sigma}\}$. Neural quantum states (NQS) approach this by using a neural network to represent such a tunable function $\psi_{\theta}(\sigma)$ which maps each basis state σ to an output A_{θ}^{σ} :

$$\psi_{\theta} : \{-1, 1\}^L \longrightarrow A_{\theta} \subseteq \mathbb{C} \quad \text{with } |A_{\theta}| \leq 2^L, \quad (2)$$

where A_{θ} is the subset of \mathbb{C} that contains all wave function coefficients $\{A_{\theta}^{\sigma}\}$. For a trained model, the normalized set $\frac{A_{\theta}}{\|A_{\theta}\|_2}$ is expected to approximate the wave function of the desired state $\frac{A_{\theta}}{\|A_{\theta}\|_2} \approx \psi_{\text{state}}$. However, there is no guarantee that there exists a non exponentially scaling set of parameters θ such that the function $\psi_{\theta}(\sigma)$ represents the desired quantum state exactly or even approximately. In the following, we analyze the general structure

of NQS based on the mathematical framework of Boolean functions and investigate the underlying requirements on network architectures to represent quantum states.

III. QUANTUM STATE CHARACTERIZATION VS. REPRESENTATION

It is well-established that conventional phases of matter can be probed and characterized using local observables. For instance, in Ising systems, magnetization serves as a key local observable that reveals information about the underlying phase.

This concept of characterizing a quantum state based on local information can also be found in machine learning. Following the ideas of interpretability, many articles [40–43] showed an efficient phase detection by considering a small number of low-order correlations within the system.

Similarly, one can ask a network which and how many correlations it needs to represent a quantum state. At first glance, one might assume that the highest order contributing when representing a quantum state is the same as the one required to characterize it. Although these two tasks appear related, their required structure is inherently different.

For clarity, when discussing correlations, we refer to products over spins within one sample σ , as opposed to expectation values of correlators such as $\langle \hat{S}_i^z \hat{S}_j^z \rangle$.

For a neural quantum state, the neural network maps a basis configuration σ to a wave function coefficient $\psi_{\theta}(\vec{\sigma})$ through a combination of linear operations and applications of non-linear activation functions. The non-linear activation functions in principle enable contributions of arbitrarily high orders of correlation functions between the inputs (e.g. between $\hat{\sigma}_i^z$ at different lattice sites). Even when performing a Taylor expansion of the neural network architecture around a point \vec{p} :

$$\psi_{\theta}(\vec{\sigma}) = \sum_{n=0}^{\infty} \frac{\psi_{\theta}^{(n)}(\vec{p})}{n!} (\vec{\sigma} - \vec{p})^n, \quad (3)$$

one might also expect main contributions from lower correlation orders. Here, $\psi_{\theta}(\vec{\sigma})$ can be any arbitrary network architecture with weights θ and a converging Taylor series. The $1/n!$ in the Taylor series suppresses higher-order terms by construction, as required for convergence. Therefore, one might conclude from working NQS examples that only lower-order correlations play a significant role. In the following, we will show that this is not necessarily the case. We first show numerical results obtained by using a correlator transformer architecture, and then explain the findings based on the mathematical framework of Boolean functions.

Correlator Quantum States.— The idea that any network architecture can be expanded using Taylor series (at least locally), makes a correlator neural network

[40, 42, 43] that simulates the Taylor expansion up to some order n , a valuable tool to acquire information about the required network structure. In our study, we analyze the structure by changing the maximal accessible expansion (correlation) order n . We define the highest expansion (correlation) order n by all $\binom{L}{n}$ correlations $\mathcal{X}_S(\vec{\sigma})$:

$$\mathcal{X}_S(\vec{\sigma}) = \prod_{i \in S} \sigma_i, \quad (4)$$

with $|S| = n$. Note that S is a set of n out of L sites i that specifies the product of spins σ_i within a spin configuration $\vec{\sigma}$.

To numerically investigate the dependence of NQS on correlations $\mathcal{X}_S(\vec{\sigma})$, we employ the correlator transformer architecture proposed in Suresh et al. [42]. A detailed description is provided in the Appendix A.

The main idea of this transformer is to operate without standard non-linear activation functions, and to instead employ the non-linearity of higher-order correlations within a snapshot. These correlations are weighted and then used to evaluate the desired system. Based on the model's performance, one can infer the importance of different correlation order.

In the context of NQS, the correlator quantum state (CQS) wave function is defined as:

$$|\psi\rangle = \sum_{\vec{\sigma}} \psi(\vec{\sigma}) |\vec{\sigma}\rangle \quad \text{with} \quad \psi(\vec{\sigma}) = W^{\text{pred}} \mathbb{X}(\vec{\sigma}) + \beta, \quad (5)$$

where \mathbb{X} contains all correlation matrices $\mathbb{X} = [\bar{X}^1, \bar{X}^2, \dots, \bar{X}^i, \dots, \bar{X}^n]$. Each entry of \bar{X}^i contains a weighted sum over all correlation orders j of the same parity with $j \leq i$. To simplify the interpretation, we solely focus on real valued weights and wave function coefficients.

In the following, we apply the real valued correlator transformer NQS (CQS) to learn the ground state of the Ising model and the perturbed toric code. To probe the representational requirements of NQS for these systems, we vary the highest accessible correlation order n . The CQS C_n with maximal order n then contains all possible correlations up to and including order n , which we informally write as:

$$C_n = \sum_{i=0}^n \sum_{S \subseteq [L]} \mathcal{X}_S(\vec{\sigma}) \delta_{|S|,i}, \quad (6)$$

where $[L]$ denotes the set of all possible sites in the system. The resulting convergence of the energy is shown in Fig. 1 a) for the Ising model and b) for the perturbed toric code, respectively.

First, we show that our observations contradict naive expectation; then we explain our results by using the existing mathematical framework of Boolean functions.

Ising model.— We start by applying the correlator transformer NQS (CQS) to the Ising model:

$$\hat{H}_{\text{Ising}} = \sum_{\langle i,j \rangle} \hat{\sigma}_i^z \hat{\sigma}_j^z, \quad (7)$$

where σ^α are the standard Pauli operators. We define our system in the σ^z -basis. This Hamiltonian has two-body interactions and the emergent ground state phases are fully characterized by first- and second-order correlations. Even with machine learning, these correlations are sufficient to characterize the phases [42, 43].

As shown in Fig. 1 a), which plots the energy convergence of different correlator NQS C_n , the correlator transformer architecture requires access to all correlation orders to obtain the optimal results. Therefore, a quantum many-body wave functions do not generally fall off at high correlation orders. Note that poor performance of our CQS for lower correlation orders cannot be ruled out a priori, as the ansatz may be unable to represent the state or to find the optimal parameters. To exclude convergence or expressivity issues of the NQS, we also computed the exact lowest energy for the respective maximal correlation order C_n . The minimal energies are displayed as horizontal lines in Fig. 1 a). Note that this was achieved by rotating the Hamiltonian into the correlator basis given in Eq. (14).

While $C_1 = \mathcal{X}_\emptyset + \mathcal{X}_{|S|=1} = \text{bias} + \text{order 1}$ completely fails to converge to the antiferromagnetic (AFM) ground state, C_8 , which includes correlations up to 8th order, achieves better results. However, the relative error remains at approximately $\epsilon \approx 10\%$. A further increase in the order of correlations significantly improves the results. With C_{11} , the relative error is reduced to approximately $\epsilon \approx \mathcal{O}(10^{-2})$. However, the best performance, $\epsilon \approx \mathcal{O}(10^{-3})$, is achieved only when all correlation orders are included ($C_L = C_{16}$). From the naive perspective, this is unexpected, as even C_8 and C_{11} , that contain all correlations up to order 8, 11 respectively, still fail to fully represent the antiferromagnetic ground state.

We emphasize the importance of this finding: The AFM state is a product state - the simplest form of a quantum state. While it is trivial to encode this state as a Matrix Product State with bond dimension 1, NQS (in the $|\vec{\sigma}_z\rangle$ basis) requires all L correlation orders (C_L) in the system. Note that this does not imply that product states are fundamentally hard for NQS to represent, just that the amount of information needed to do so can be of order system size.

In Section VII we explain our findings based on a mathematical framework. For instance, it can be shown analytically that the correlation order 16 is (for the AFM ground state) a significant contribution to the wave function.

Toric code model.— We now turn to the perturbed toric code model, which is, for our study, particularly interesting, as it exhibits topological order due to four-

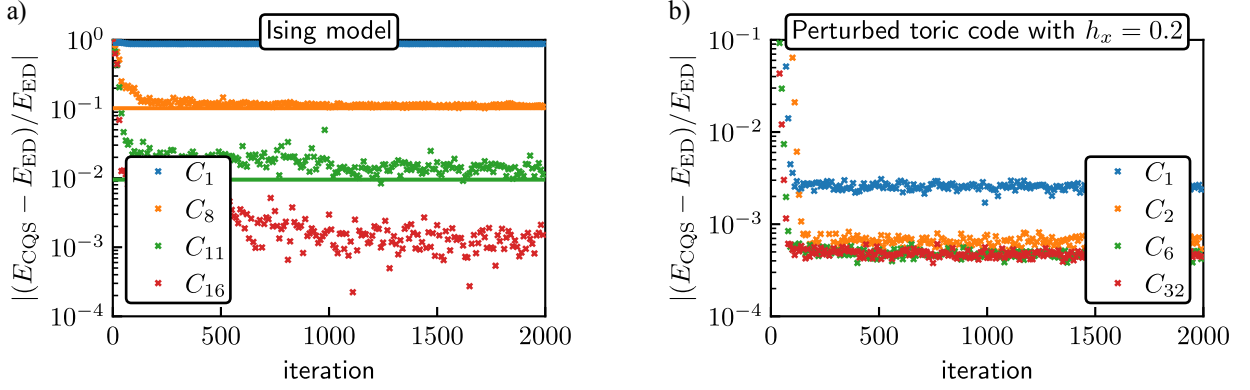


FIG. 1. Convergence of the correlator transformer (square lattice of linear size $L = 4$) applied to (a) the Ising model and (b) the perturbed toric code. C_n defines a network that uses all correlations up to order n . The horizontal lines shown in (a) are the (exact) lowest possible energies for the respective maximal correlation order. The exact energies in the correlator basis were calculated using Eq. (17).

body interactions. The corresponding Hamiltonian is defined by:

$$\hat{H}_{\text{TC}} = - \sum_j \prod_{i \in +_j} \hat{\sigma}_i^x - \sum_j \prod_{i \in \square_j} \hat{\sigma}_i^z + h_x \sum_i \hat{\sigma}_i^x. \quad (8)$$

Again, σ^α are the usual Pauli operators. We define the spins in the system as the connecting links between sites, such that the total Hilbert space dimension is given by $2^{2(L_x \times L_y)}$. For the NQS simulation, we choose to constrain the Hilbert space to the physical sector where Gauss's law:

$$G_i = \prod_{j \in +_i} \hat{\sigma}_j^x \stackrel{!}{=} 1 \quad (9)$$

is always fulfilled, thus reducing the effective Hilbert space to $2^{(L_x \times L_y)+1}$ [44, 45]. This is achieved by choosing the σ^x -basis as the computational basis, which allows to restrict the Monte Carlo updates to states from the physical sector.

The perturbed toric code is a Hamiltonian with a topological phase, which makes it, in principle, difficult to characterize the relevant information for a given phase or wave function. For phase detection tasks, it was shown that 4th order correlations are sufficient to achieve a successful classification [42]. Similar to the Ising model, one can show that an NQS requires all correlations in the system if one works in the full Hilbert space (see Section VII). However, in the considered case with a Hilbert space truncation, it is at first unclear which and how many correlations are required for a full description.

Note that if we enforce Gauss's law, the limiting case of the pure toric code model ($h_x = 0$) has a trivial solution, which is given by a constant $\psi_{\text{res}}^{h_x=0}(\vec{\sigma}) = C_0$.

In Fig. 1b), we show the convergence of the correlator transformer model for the perturbed toric code with $h_x = 0.2$. One immediately notices that the perturbed

toric code, despite the topologically ordered phase, is significantly easier to learn than the AFM ground state. All evaluated correlator transformers achieve a reasonable error of $\epsilon \lesssim \mathcal{O}(10^{-3})$. This can be attributed to the fact that the system at $h_x = 0.2$ remains in the topologically ordered phase, so that only minor deviations from the unperturbed ground state $\psi_{\text{res}}^{h_x=0}(\vec{\sigma}) = C_0$ are expected.

While C_1 , which contains first-order correlations and a bias, already achieves a reasonable error of $\epsilon \approx \mathcal{O}(10^{-3})$, the results can still be improved by providing access to higher-order correlations. However, already when using C_6 , an optimization limit is reached, where we do not observe any further improvement when increasing the number of accessible correlation orders. Even when access to all correlations is allowed in C_{32} , we do not observe a major difference in the convergence or the energy errors.

Although a generally good performance of the NQS for the slightly perturbed toric code with enforced Gauss's law is expected, the stagnation observed for $C_{\geq 6}$ is surprising, given that the number of correlations accessible to the C_{32} NQS is several orders higher than those available to the C_6 NQS (compare with Eq. (16)). In Section VII, we explain the reduced number of required correlations using the decision tree formalism described in Sec. V and demonstrate that Gauss's law introduces linear dependencies, and thus reduces the order of correlation needed to represent the ground state.

Remark. — The best energies that we obtained in the training are limited by the representational power of our network architecture. However, the correlator transformer was built to yield interpretability at the cost of reduced complexity. Together with the limited number of parameters, which we set to $\#\text{params} \approx \mathcal{O}(2 \times 10^4)$ for all correlator NQS simulations, we do not expect a perfect convergence.

IV. ANALYSIS OF FUNCTIONS WITH BINARY INPUTS

While neural quantum states are often perceived as a purely “black box” technique, we show that a much better understanding of the working principle can be achieved when studying the underlying structure. To do so, we follow the mathematical framework of Boolean functions [46]. Note that there is an extension of this framework to higher local Hilbert space dimensions and to one-hot encoding. We comment on these generalizations in Appendix B.

The analysis of real valued Boolean functions $\psi : \{-1, 1\}^L \rightarrow \mathbb{R}$ is based on studying their Fourier expansion. The Fourier expansion can be readily derived by introducing an indicator polynomial:

$$1_{\vec{\alpha}}(\vec{\sigma}) = \frac{(1 + \alpha_1 \sigma_1)}{2} \dots \frac{(1 + \alpha_L \sigma_L)}{2} = \begin{cases} 1, & \vec{\sigma} = \vec{\alpha}, \\ 0, & \vec{\sigma} \neq \vec{\alpha}. \end{cases} \quad (10)$$

This indicator function is a multilinear polynomial that includes correlations up to L^{th} order. Consequently, any wave function of a finite-size spin system has a polynomial representation of the form:

$$\psi(\vec{\sigma}) = \sum_{\vec{\alpha} \in \{-1, 1\}^L} \psi(\vec{\alpha}) 1_{\vec{\alpha}}(\vec{\sigma}) \quad (11)$$

Rewriting this polynomial representation in terms of all possible (overlapping) subsets S of $[L] = [\sigma_1, \sigma_2, \dots, \sigma_L]$ yields the Fourier representation of $\psi(\vec{\sigma})$:

$$\psi(\vec{\sigma}) = \sum_{S \subseteq [L]} \langle \vec{\sigma} | \mathcal{X}_S \rangle \langle \mathcal{X}_S | \psi \rangle = \sum_{S \subseteq [L]} \bar{\psi}(S) \mathcal{X}_S(\vec{\sigma}), \quad (12)$$

where the corresponding Fourier coefficients are defined as:

$$\bar{\psi}(S) = \langle \mathcal{X}_S | \psi \rangle = \frac{1}{2^L} \sum_{\vec{\sigma} \in \{-1, 1\}^L} \psi(\vec{\sigma}) \mathcal{X}_S(\vec{\sigma}), \quad (13)$$

and the monomial $\mathcal{X}_S(\vec{\sigma})$ corresponding to S is given by:

$$\mathcal{X}_S(\vec{\sigma}) = \langle \vec{\sigma} | \mathcal{X}_S \rangle = \prod_{i \in S} \sigma_i, \quad (14)$$

with $\mathcal{X}_{\emptyset}(\vec{\sigma}) = 1$. This construction yields in total 2^L monomials that form an orthonormal basis for the $H_{\text{dim}} = 2^L$ dimensional Hilbert space [46]:

$$\langle \mathcal{X}_S | \mathcal{X}_T \rangle = \frac{1}{2^L} \sum_{\vec{\sigma} \in \{-1, 1\}^L} \mathcal{X}_S(\vec{\sigma}) \mathcal{X}_T(\vec{\sigma}) = \begin{cases} 1, & S = T, \\ 0, & S \neq T. \end{cases} \quad (15)$$

Note that the k^{th} correlation order (all S of the same degree: $|S| = k$) contributes $\frac{L!}{k!(L-k)!}$ monomials to the basis. Thus, a CQS C_n with correlations up to n^{th} order has access to $N(C_n)$ basis vectors:

$$N(C_n) = \sum_{k=0}^n \frac{L!}{k!(L-k)!} = \sum_{k=0}^n \binom{L}{k} \stackrel{n=L}{=} 2^L. \quad (16)$$

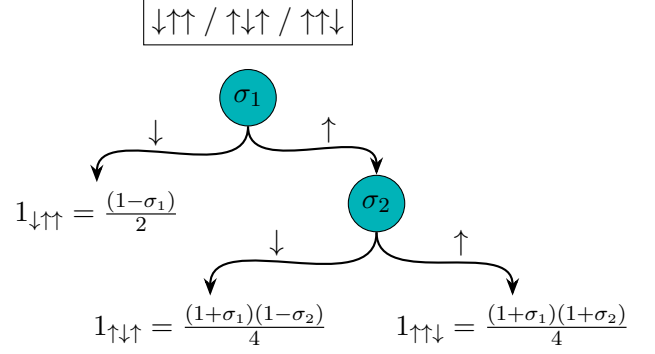


FIG. 2. Decision tree for a three spin model with a fixed magnetization of $\langle \sum_i \sigma_z^i \rangle = 1$.

Consequently, ground states (GS) of Hamiltonians:

$$\hat{H} = \sum_{S, S' \subseteq [L]} \underbrace{\left(\frac{1}{2^L} \sum_{\vec{\sigma}, \vec{\sigma}'} \langle \mathcal{X}_S | \vec{\sigma} \rangle h_{\vec{\sigma}, \vec{\sigma}'} \langle \vec{\sigma}' | \mathcal{X}_{S'} \rangle \right)}_{h_{S, S'}} |\mathcal{X}_S\rangle \langle \mathcal{X}_{S'}|, \quad (17)$$

with relevant contributions $h_{R, S'}$ in higher-order correlations $|R| > n$, such that $\bar{\psi}_{\text{GS}}(R) \neq 0$, cannot be fully represented by the CQS C_n for $n < |R| \leq L$. Here, $h_{\vec{\sigma}, \vec{\sigma}'}$ is the usual matrix element $h_{\vec{\sigma}, \vec{\sigma}'} = \frac{1}{2^L} \langle \vec{\sigma} | \hat{H} | \vec{\sigma}' \rangle$. Note that due to the normalization of $\langle \mathcal{X}_S | \mathcal{X}_T \rangle = \delta_{S, T}$ we used the convention $\langle \vec{\sigma} | \vec{\sigma}' \rangle = 2^L \delta_{\vec{\sigma}, \vec{\sigma}'}$ and $\mathbb{1} = \frac{1}{2^L} \sum_{\vec{\sigma} \in \{-1, 1\}^L} |\vec{\sigma}\rangle \langle \vec{\sigma}|$.

Remark.— We want to stress the importance of this formalism for neural quantum states: Eq. (12) decouples the influence of the network weights, included in $\bar{\psi}(S)$, from the input configuration, given in $\mathcal{X}_S(\vec{\sigma})$. In other words, the machine learning algorithm approximates the quantum state in the correlator basis $|\mathcal{X}_S\rangle$ and rotates it into the desired spin basis:

$$|\psi\rangle = \sum_{S \subseteq [L]} \bar{\psi}(S) |\mathcal{X}_S\rangle \Rightarrow \sum_{\vec{\sigma} \in \{-1, 1\}^L} \sum_{S \subseteq [L]} \bar{\psi}(S) \langle \vec{\sigma} | \mathcal{X}_S \rangle |\vec{\sigma}\rangle \quad (18)$$

Therefore, we can think of the correlator basis $|\mathcal{X}_S\rangle$ as the internal basis that neural quantum states use for quantum state representation. Consequently, seemingly simple things, such as setting wave function coefficients $\psi(\vec{\sigma})$ to zero can become a difficult task for NQS-like quantum state representation, as this requires combinations of potentially non-trivial $\bar{\psi}(S)$.

V. DECISION TREE

Although the Fourier expansion described above provides a good starting point for the analysis, it becomes challenging to understand the behavior of NQS in systems with artificially reduced Hilbert spaces, such as fixed magnetization, Gauss’s law, or particle conservation. To address this, one can introduce a decision tree

representation (see Fig. 2). Similar to autoregressive NQS models [47, 48], this approach constructs paths through the lattice and sequentially checks for allowed (disallowed) local spin configurations. Following this, the restricted wave function ψ_{res} can be written as:

$$\psi_{\text{res}}(\vec{\sigma}) = \sum_{\vec{p} \in T} \psi(\vec{p}) 1_{\vec{p}}^{\text{res}}(\vec{\sigma}), \quad (19)$$

where \vec{p} denotes a valid path in the decision tree T . Again, $1_{\vec{p}}^{\text{res}}(\vec{\sigma})$ is an indicator polynomial built from $\frac{(1+p_i\sigma_i)}{2}$ elements. Once a branch in the tree becomes trivial (e.g. all particles are distributed), this polynomial ends.

In the context of the Fourier (or Taylor) expansion, the restriction of the Hilbert space reduces the maximal correlation order in the Fourier representations to the maximal length of a branch $\max |\vec{p}|$ (compare with Fig. 2). Importantly, due to the truncation of the Hilbert space, many of the monomials \mathcal{X}_S become linearly dependent, which implies that the Fourier basis loses (at least partially) its orthogonality: $\max |\vec{p}| \geq \dim(\mathcal{H}_{\text{space}}^{\text{res}})$.

So far, we have considered only one single decision tree. However, decision trees are not unique. Therefore, one can sum over all possible decision trees $\mathbb{T} = [T_1, T_2, \dots]$ for each configuration and select the path with minimal depth to the desired state:

$$\psi_{\text{res}}(\vec{\sigma}) = \sum_{\min |\vec{p}| \in \mathbb{T}} \psi(\vec{p}) 1_{\vec{p}}^{\text{res}}(\vec{\sigma}). \quad (20)$$

For the three-spin example with a fixed magnetization of $\langle \sum_i \hat{\sigma}_z^i \rangle = 1$, shown in Fig. 2, this is equivalent to choosing:

$$1_{\downarrow\uparrow\uparrow} = \frac{(1 - \sigma_1)}{2}, 1_{\uparrow\downarrow\uparrow} = \frac{(1 - \sigma_2)}{2}, 1_{\uparrow\uparrow\downarrow} = \frac{(1 - \sigma_3)}{2}. \quad (21)$$

Note that σ_3 is constrained by $\sigma_3 = 1 - (\sigma_1 + \sigma_2)$.

VI. INTUITIVE APPROACH TO FOURIER EXPANSION

In Sec. IV and Sec. V, we showed formally that every function $\psi : \{-1, 1\}^L \rightarrow \mathbb{R}$ can be written as a Fourier expansion [46]. Here, we provide a more intuitive picture of what this means for neural quantum states.

Writing out the Fourier expansion of a wave function $\psi(\vec{\sigma})$ explicitly reveals its structure:

$$\begin{aligned} \psi(\vec{\sigma}) = & W + \sum_i A_i \sigma_i + \sum_{j < i} B_{ij} \sigma_i \sigma_j + \dots \\ & + F \sigma_1 \sigma_2 \sigma_3 \dots \sigma_L, \end{aligned} \quad (22)$$

where each variable (W, A_i, B_{ij}, \dots, F) correspond to a specific Fourier coefficient $\psi(S)$. Notice the similarity to

a Taylor expansion. Writing the wave function coefficient $\psi(\vec{\sigma})$ for each basis state yields a set of 2^L equations:

state	$\psi(\sigma)$
$ \uparrow\uparrow\uparrow \dots \uparrow\rangle$	$A_1 + A_2 \dots + B_{12} + B_{13} \dots + F \dots + W$
$ \uparrow\uparrow\downarrow \dots \uparrow\rangle$	$A_1 - A_2 \dots - B_{12} - B_{13} \dots - F \dots + W$
\vdots	\vdots
$ \uparrow\downarrow\downarrow \dots \downarrow\rangle$	$A_1 - A_2 \dots - B_{12} - B_{13} \dots \mp F \dots + W$
$ \downarrow\downarrow\downarrow \dots \downarrow\rangle$	$-A_1 - A_2 \dots + B_{12} + B_{13} \dots \pm F \dots + W$

(23)

The signs in front of the coefficients reflect the products of spins in that state. Importantly, the parity of the prefactor of F , $\sigma_1 \sigma_2 \sigma_3 \dots \sigma_L = \pm 1$, changes with the number of lattice sites.

The task we aim to achieve with neural quantum states is solving these 2^L linearly independent equations, which generally requires all 2^L Fourier coefficients A_i, B_{ij}, \dots , so we cannot arbitrarily assume that some coefficients are negligible. Note that setting coefficients of higher-order correlations to zero is equivalent to overdetermining the system, which can, depending on the quantum state, prevent an exact solution and make approximations difficult, if not impossible.

From this perspective, the Fourier representation provides a natural language to understand the requirements for neural quantum states. The network must be able to generate the set of correlations needed to represent the wave function. Whether this requires all orders or only a truncated subset depends on both the quantum state and the choice of computational basis, as we discuss in later sections.

VII. EXPLAINING OBSERVATIONS BASED ON MATHEMATICAL FRAMEWORK

Based on the mathematical framework introduced in Sec. IV and Sec. V, we now analyze the numerical observations made in Sec. III. We begin with the Ising model and thereafter turn to the perturbed toric code.

Ising model. — In our numerical experiments, we found that all correlation orders are required to obtain a good ground state representation for a classical Ising model. At first glance, this may seem counterintuitive considering that the characterization of an antiferromagnetic state can be achieved by local measurements. However, with the framework discussed in Sec. IV, we can now prove that the highest-order Fourier coefficient $\bar{\psi}(L)$ is a relevant contribution to the ground state.

Note that we restrict this explanation to positive wave function coefficients $\psi(\sigma) \geq 0$ with an even number of spins. Depending on the parity of the number of lattice sites and the sign structure of the ground state, the highest contributing correlation order can shift to $L - 1$ such that $\bar{\psi}(L - 1) \geq \bar{\psi}(S)$.

Starting from Eq. (13), we see that the number of down spins in the subset S of the contributing basis states de-

termines the magnitude of the Fourier coefficient. For an antiferromagnetic (AFM) state we obtain:

$$\begin{aligned}\bar{\psi}_{\text{AFM}}(S) &= \frac{1}{2^L} \sum_{\vec{\sigma} \in \{-1,1\}^L} \psi_{\text{AFM}}(\vec{\sigma}) \prod_{i \in S} \sigma_i \\ &= \frac{1}{2^L} \left[\psi_A \prod_{i \in S} \sigma_i^A + \psi_B \prod_{i \in S} \sigma_i^B \right]\end{aligned}\quad (24)$$

Here, we used A and B for the two possible AFM states. In the considered 4×4 Ising model the AFM ground states contain an even number of down spins, implying that the two corresponding highest order monomials are $\mathcal{X}_L(\text{even} \downarrow) = 1$. Plugging this into Eq. (24) we obtain:

$$\bar{\psi}(L) = \frac{1}{2^L} (\psi_A + \psi_B) \geq \bar{\psi}(S), \quad (25)$$

for any $S \subseteq [L]$, which makes the highest correlation order (for positive wave function coefficients) a significant contribution to the wave function. Therefore, the correlator transformer that was used for the Ising model in Sec. III with C_8 and C_{11} cannot represent the full ground state although it has access to approximately 60% and 96% of all correlations (compare with Eq. (16)), respectively.

Note that the general form of the Fourier coefficients for an AFM state can be derived using Eq. (24):

$$\bar{\psi}(S) = \begin{cases} \pm \frac{1}{2^L} [\psi_A + \psi_B] & \text{for } |S| = \text{even}, \\ \pm \frac{1}{2^L} [\psi_A - \psi_B] & \text{otherwise,} \end{cases} \quad (26)$$

which shows that higher-order correlations are as relevant as lower correlation orders of the same parity. The large number of non-zero coefficients $\bar{\psi}(S)$ arises because the network must set most wave function coefficients $\psi_{\text{AFM}}(\vec{\sigma})$ to zero.

Remark.— This analysis can be readily extended to other quantum states constructed from basis states $|\vec{\sigma}\rangle$ with an even number of down spins. The toric code ground state in the full Hilbert space is an example of a more complex quantum state that shows the same behavior $\bar{\psi}_{\text{TC}}(L) \geq \bar{\psi}_{\text{TC}}(S)$.

Toric code model.— The numerical simulation of the perturbed toric code model with enforced Gauss's law (compare with Fig. 1b) revealed that only a limited number of correlation orders played a significant role in obtaining the best possible ground state energy.

The Hilbert space of the toric code model restricted to the physical sector has dimension $2^{L_x \times L_y + 1}$ [44, 45], which means the system of equations is underdetermined (compare with Sec. VI). Following the spanning tree formalism (see App. C), an orthogonal basis can be constructed from $L_x \times L_y + 1$ linearly independent spins. These spins uniquely determine the remaining $L_x \times L_y - 1$ spins, fully specifying the state within the physical subspace. Therefore, using a decision tree (as described in Sec. V) that includes precisely these $L_x \times L_y + 1$ spins, is

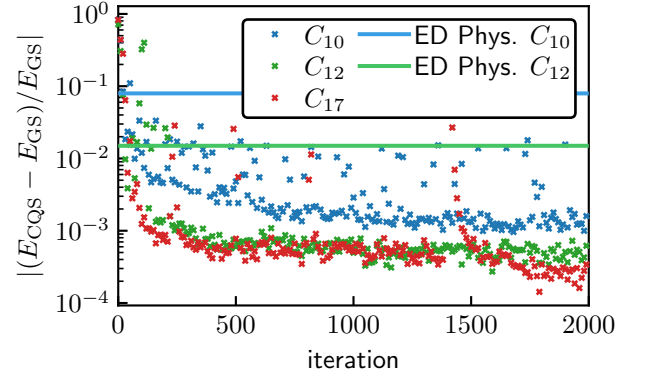


FIG. 3. Convergence of the CQS (access to all sites) for the perturbed toric code (4×4) model with enforced Gauss's law ($h_x = 1$ and star and plaquette term set to zero). We compare the CQS to exact diagonalization results (horizontal lines) in the correlation basis with correlations up to order 10 (blue) and 12 (green).

sufficient for an exact representation of the physical sector. However, this construction requires capturing correlations up to order $L_x \times L_y + 1$. Despite this, the results shown in Fig. 1b indicate that lower-order correlations already suffice for an accurate approximation of the ground state $\psi_{\text{res}}^{h_x=0.2}$.

One might argue that higher-order correlations are not essential in this regime, especially since $\psi_{\text{res}}^{h_x=0.2}$ remains close to the uniform $h_x = 0$ ground state $\psi_{\text{res}}^{h_x=0.0} = C_0$. To investigate this matter, we now consider the large h_x limit. In the previous analysis it was shown that representing the ferromagnetic ground state $|++\dots+\rangle$ in the σ^x -basis (large h_x limit) requires all $(L_x \times L_y + 1)$ correlation orders in the reduced Hilbert space.

Fig. 3 shows the convergence of the CQS (with access to all sites) for various maximal correlation orders in the large h_x limit. Furthermore, we compare the CQS energy to exact results obtained by diagonalizing the Hamiltonian in the orthogonal correlator basis (up to some correlation order) of the $L_x \times L_y + 1$ linearly independent spins. Similarly to the behavior observed in Fig. 1b), we notice that the results, beyond a certain correlation order, do not improve further. All tested CQS obtain a minimal relative error of $\epsilon \approx \mathcal{O}(10^{-3})$. Furthermore, considering the same maximal correlation order, the CQS surpasses the exact results by several magnitudes. Here, the sole advantage of the CQS is the additional information about the remaining $L_x \times L_y - 1$ spins. Consequently, we can conclude that the information about the predetermined $L_x \times L_y - 1$ spins has to contain higher-order correlations of the $L_x \times L_y + 1$ linear independent spins so that accurate results can be obtained even when not considering all $L_x \times L_y + 1$ correlation orders.

This is equivalent to saying that the spanning tree and therefore the decision tree in this toric code model is not unique. While we chose a specific decision tree for the exact diagonalization with a maximum correlation order

of $L_x \times L_y + 1$, we allowed the CQS to choose the shortest and most efficient path.

Remark.— We emphasize that the exact diagonalization (compare with Fig. 3) only uses states from the physical sector and is, therefore, still feasible for 32 spins.

VIII. CHOOSING THE COMPUTATIONAL BASIS

In the research of neural quantum states, the problem of how to choose the most suitable reference basis for a given quantum state remains unsolved. However, with the framework introduced above, we can intuitively draw conclusions about the desired NQS structure, which provides insights about potential difficulties for the quantum state representation.

The internal NQS structure can be analyzed by rotating the variational wave function in the correlator basis:

$$\psi(\vec{\sigma}) = \sum_{S \subseteq [L]} \bar{\psi}(S) \mathcal{X}_S(\vec{\sigma}). \quad (27)$$

Importantly, the coefficients $\bar{\psi}(S)$ depend solely on the variational parameters and not on the input configuration and are therefore a direct consequence of the network's parameters and structure (see Sec. IV). To determine whether the network must learn a relatively simple or complex structure of coefficients $\bar{\psi}(S)$, it is necessary to identify known patterns or similarities.

To do so, we revisit Eq. (17). In this equation we show the rotation of the Hamiltonian from the spin basis $|\sigma\rangle$ to the correlation basis $|\mathcal{X}_S\rangle$:

$$\hat{H} = \underbrace{\frac{1}{2^L} \sum_{\vec{\sigma}, S} \langle \mathcal{X}_S | \vec{\sigma} \rangle \langle \vec{\sigma} |}_{\mathcal{X}} \hat{H} \underbrace{\frac{1}{2^L} \sum_{\vec{\sigma}', S'} \langle \vec{\sigma}' | \mathcal{X}'_S \rangle \langle \mathcal{X}'_S |}_{\mathcal{X}^\dagger}. \quad (28)$$

Although this rotation matrix \mathcal{X} with matrix elements $\mathcal{X}_{S, \vec{\sigma}} = \langle \mathcal{X}_S | \vec{\sigma} \rangle$ can seem complicated, it has the simple and well known form of Hadamard matrices for spin-1/2 systems [46]:

$$\mathcal{X} = H_1 \otimes H_2 \otimes \dots \otimes H_L$$

$$\text{with } H_i = \begin{pmatrix} \mathcal{X}_{S_i=\emptyset, \uparrow} = 1 & \mathcal{X}_{S_i=i, \uparrow} = 1 \\ \mathcal{X}_{S_i=\emptyset, \downarrow} = 1 & \mathcal{X}_{S_i=i, \downarrow} = -1 \end{pmatrix} \quad (29)$$

The same basis transformation is used to rotate from $|\vec{\sigma} = \vec{\sigma}_{x/z}\rangle$ to $|\vec{\sigma}_{x/z}\rangle$.

$$U = \sum_{\vec{\sigma}_x, \vec{\sigma}_z} u_{\vec{\sigma}_x, \vec{\sigma}_z} |\vec{\sigma}_x\rangle \langle \vec{\sigma}_z| = H_1^\sigma \otimes H_2^\sigma \otimes \dots \otimes H_L^\sigma$$

$$\text{with } H_i^\sigma = \begin{pmatrix} u_{+, \uparrow} = 1 & u_{+, \downarrow} = 1 \\ u_{-, \uparrow} = 1 & u_{-, \downarrow} = -1 \end{pmatrix} \quad (30)$$

Consequently, the matrix elements $h_{n,m}^{\mathcal{X}, z/x}$ of a Hamiltonian in the correlator basis $|\mathcal{X}_S\rangle$ are the same as the

elements $h_{n,m}^{\sigma_{x/z}}$ in the $|\vec{\sigma}_{x/z}\rangle$ basis:

$$\hat{H} = \sum_{n,m=1}^L h_{n,m}^{\mathcal{X}, z/x} |n_{\mathcal{X}}\rangle \langle m_{\mathcal{X}}|$$

$$= \sum_{n,m=1}^L h_{n,m}^{\sigma_{x/z}} |n_{\sigma_{x/z}}\rangle \langle m_{\sigma_{x/z}}|, \quad (31)$$

with $h_{n,m}^{\mathcal{X}, z/x} = h_{n,m}^{\sigma_{x/z}}$. Here, $n, m \leq 2^L$ are numbers that correspond to the n^{th} basis vector in the given basis. E.g. in the $|\sigma_z\rangle$ basis, the number $n = 1$ ($n = 2^L$) corresponds to the basis state:

$$|n_{\sigma_z} = 1\rangle \equiv |\uparrow\uparrow \dots \uparrow\rangle = \bigotimes_{i=1}^L \begin{pmatrix} 1 \times |\uparrow_i\rangle \\ 0 \times |\downarrow_i\rangle \end{pmatrix} \text{ and}$$

$$|n_{\sigma_z} = 2^L\rangle \equiv |\downarrow\downarrow \dots \downarrow\rangle = \bigotimes_{i=1}^L \begin{pmatrix} 0 \times |\uparrow_i\rangle \\ 1 \times |\downarrow_i\rangle \end{pmatrix} \quad (32)$$

and in the correlator basis $|\mathcal{X}_S\rangle$ we define it as:

$$|n_{\mathcal{X}} = 1\rangle \equiv |\mathcal{X}_\emptyset\rangle = \bigotimes_{i=1}^L \begin{pmatrix} 1 \times |\mathcal{X}_{S_i=\emptyset}\rangle \\ 0 \times |\mathcal{X}_{S_i=i}\rangle \end{pmatrix} \text{ and}$$

$$|n_{\mathcal{X}} = 2^L\rangle \equiv |\mathcal{X}_L\rangle = \bigotimes_{i=1}^L \begin{pmatrix} 0 \times |\mathcal{X}_{S_i=\emptyset}\rangle \\ 1 \times |\mathcal{X}_{S_i=i}\rangle \end{pmatrix}. \quad (33)$$

Note that we purposely added the index z/x to clarify that the matrix element $h_{n,m}^{\mathcal{X}, z/x}$ contains products of single spins in the z/x basis and therefore dependent on the computational basis (σ_x or σ_z), while the corresponding elements $h_{n,m}^{\sigma_{x/z}}$ are the usual matrix elements in the respective x/z basis.

The consequence of having the same matrix elements $h_{n,m}^{\mathcal{X}, z/x} = h_{n,m}^{\sigma_{x/z}}$ is that the coefficients for the ground state wave function are the same in correlator basis $\psi^{\mathcal{X}, z/x}(n)$ and the corresponding spin basis $\psi^{\sigma_{x/z}}(n)$:

$$\psi^{\mathcal{X}, z/x}(n) = \psi^{\sigma_{x/z}}(n), \quad (34)$$

with:

$$|\Psi\rangle = \sum_{n=1}^L \psi^{\mathcal{X}, z/x}(n) |n_{\mathcal{X}}\rangle = \sum_{n=1}^L \psi^{\sigma_{x/z}}(n) |n_{\sigma_{x/z}}\rangle, \quad (35)$$

which allows to predict the difficulty for NQS simulations. Note that we use $\psi^{\mathcal{X}, z/x}(n)$ instead of $\bar{\psi}(S)$ at the n^{th} basis vector of $|\mathcal{X}_S\rangle$ for better comparability.

What does this mean and how can we profit from this?— In almost all cases, we intuitively pick the basis in which the wave function is peaked the most. E.g. the natural choice for an $|\uparrow\uparrow \dots \uparrow\rangle$ state would be the $|\sigma_z\rangle$ basis, since this provides an easy understanding of what we want to represent. However, as we showed in Sec. VII, this requires surprisingly much computational effort (all correlation orders require the same coefficient),

since it is difficult to align the weights such that most of the wave function coefficients are tuned to zero.

The analogy of correlations in the $|\vec{\sigma}_z\rangle$ basis to the wave function in the $|\sigma_x\rangle$ basis would have shown the same result. The product state $|\uparrow\uparrow\dots\uparrow\rangle$ in the $|\vec{\sigma}_x\rangle$ basis requires all wave function coefficients to be the same: $\psi^{\sigma_x}(n) = \psi^{\mathcal{X},z}(n) = C$. While the wave function in the $|\vec{\sigma}_z\rangle$ basis is peaked, the wave function in the correlator basis $|\mathcal{X}_S\rangle$ is widely spread.

If one uses the $|\vec{\sigma}_x\rangle$ basis instead, which is counterintuitive at first glance, the wave function in the correlator basis $|\mathcal{X}_S\rangle$ matches the wave function in the $|\vec{\sigma}_z\rangle$ basis and is therefore strongly peaked: $\psi^{\sigma_z}(n) = \psi^{\mathcal{X},x}(n) = \delta_{1,n}$. In a neural network, this requires just one single bias, with all other weights set to zero.

In summary, even a rough understanding of the ground state wave function in the $|\vec{\sigma}_z\rangle$ and $|\vec{\sigma}_x\rangle$ bases can provide a useful indication of which basis may lead to a wave function that is more or less peaked. Counterintuitively, choosing the reference basis where the true ground state wave function is less peaked will yield a more peaked wave function in the corresponding correlator basis. This can prove advantageous, especially when predominantly low correlation orders need to be captured by the NQS (compare with Sec. IX). However, one has to keep in mind that the sign structure also changes with the basis, which can complicate the optimization [49, 50].

Remark.— By applying unitary transformations, often in the form of Pauli operators $U_{z/x} = \prod_{i \in A} \sigma_i^{z/x}$, we can change the sign structure $\psi_{\text{NQS}}(\sigma)U_z|\sigma_z\rangle \rightarrow (-1)^{N_A^\sigma} \psi_{\text{NQS}}(\sigma)|\sigma\rangle$ (N_A^σ is the number of down spins on the sublattice A) and the order of the basis states $\psi_{\text{NQS}}(\sigma)U_x|\sigma_z\rangle \rightarrow \psi_{\text{NQS}}(\sigma)|-\sigma_z^A\rangle \otimes |\sigma_z^{\bar{A}}\rangle$. This can, in many cases, help to construct a basis that reduces the requirements of the NQS wave function.

IX. COMPARING TO TAYLOR EXPANSION

In neural quantum states, a machine learning algorithm is trained such that it can represent a quantum state. In the previous sections, we addressed the topic of representability based on the information (correlations) that the algorithm might (not) have access to. While we know that there exists a polynomial description of the desired quantum state, it is unclear if the used machine learning algorithm can represent this polynomial. In the following, we study the requirements for an algorithm to extract the given information or to potentially simplify the optimization problem by using locally analytic activation functions.

To do so, we focus on the Taylor expansion of a function $\psi(\vec{\sigma})$ around point \vec{p} :

$$\psi(\vec{\sigma}) = \sum_{n=0}^{\infty} \frac{\psi^{(n)}(\vec{p})}{n!} (\vec{\sigma} - \vec{p})^n. \quad (36)$$

Based on the Taylor series, we address the role of a bias,

potential problems with shallow networks, and the effects of activation functions with nonanalyticities.

Even and odd orders: The role of the bias.— As shown in Sec. IV, any wave function of a finite size spin system can be described as a combination of even and odd orders of correlations: $\psi(\sigma) = Y_{\text{even}}(\sigma) + Y_{\text{odd}}(\sigma)$. While even orders are spin symmetric ($Y_{\text{even}}(\sigma) = Y_{\text{even}}(-\sigma)$), odd orders are antisymmetric ($Y_{\text{odd}}(\sigma) = -Y_{\text{odd}}(-\sigma)$). Therefore, the quantum states with an even (odd) parity (i.e. a ground state of the Ising model), can be represented by solely using even (odd) correlations. On the other hand, systems that are not spin symmetric $|\psi(\sigma)| \neq |\psi(-\sigma)|$ require both even and odd orders.

While this is not surprising, one has to keep in mind that many frequently used activation functions do have a fixed parity:

$$\begin{aligned} \sinh(x) &= -\sinh(-x), \\ \cosh(x) &= +\cosh(-x), \\ \tanh(x) &= -\tanh(-x), \\ \arctan(x) &= -\arctan(-x), \\ &\vdots \\ \frac{1}{2} - \text{sigmoid}(x) &= -\left(\frac{1}{2} - \text{sigmoid}(-x)\right). \end{aligned} \quad (37)$$

Therefore, network architectures that maintain the parity of these activation functions cannot represent quantum states with a different parity. Note that the Taylor expansion of functions with even (odd) parity exclusively contains correlations of even (odd) order. To illustrate this we apply different network architectures to the in Sec. III introduced perturbed toric code model, where Gauss's law is enforced in the sampling. In Fig. 4a) we show the convergence of a single layer feed forward NQS with different activation functions (cosh, sinh, and sigmoid) and compare them to the correlator transformer with access to either purely even (C_2^{even}), odd (C_3^{odd}) or 0th + odd order (C_1) correlations. Although all NQS do not fully capture the ground state, the behavior of the activation functions can be understood very well by comparing them to the CQS, as those resemble their low expansion orders ($\cosh \approx C_2^{\text{even}}$, $\sinh \approx C_3^{\text{odd}}$, $\text{sigmoid} \approx C_1$). Since increasing the correlation order of just one parity does not improve the result (the activation functions contain all orders of one parity), we can attribute the inability to converge to the absence of interplay between even and odd correlations.

Although this may appear to restrict the use of certain activation functions in most models, these limitations can be easily overcome by introducing a bias in the neural network layer. The bias enables the presence of odd (even) correlation orders in an otherwise even (odd) order of the Taylor expansion, making it not merely a convenient optimization parameter, but a crucial component for an accurate quantum state representation.

Globally analytic NQS.— Entire functions can be fully represented by a Taylor series. By the definition of a

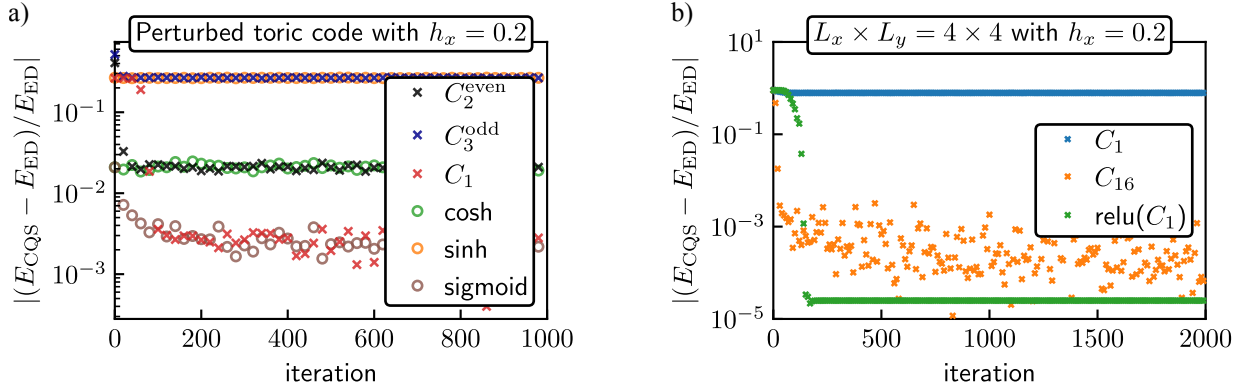


FIG. 4. Convergence of NQS models applied to (a) the perturbed toric code (Gauss’s law enforced in the sampling) and (b) the transverse field Ising model. In (a) we show a comparison between several CQS and a single layer FFNN with different activation functions. The CQS resemble low-order expansions of the corresponding activation functions ($\cosh \approx C_2^{\text{even}}$, $\sinh \approx C_3^{\text{odd}}$, $\text{sigmoid} \approx C_1$). In (b), we compare the CQS (C_1 and C_{16}) to a single layer FFNN (equivalent to C_1) with rectified linear unit activation function.

converging Taylor series, the term $\frac{1}{n!}$ suppresses higher expansion orders, which opposes the fact that the coefficient of the highest correlation order $\bar{\psi}(L)$ is important for a correct representation and sometimes even the largest coefficient: $\bar{\psi}(L) \geq \bar{\psi}(S)$ (compare with Section VII). In practice, this mismatch forces the network to generate large parameter values in order to amplify the contributions from higher-order correlations. While this achieves large coefficients for higher-order correlations, it potentially comes with a drawback: stochastic reconfiguration, which is based on linearized time evolution, is designed for small steps in both the time evolution and the parameter manifold. Therefore, large weights can slow down the accurate optimization. However, we assume that this is primarily a problem for shallow networks, as deeper neural networks struggle less with generating higher correlation orders.

As an example, consider representing an $|\uparrow\uparrow \dots \uparrow\rangle$ state ($|\sigma_z\rangle$ -Basis) with a simple single layer feed forward neural network and a cosh activation function. An exact representation of this simple product state would require infinitely large network parameters W_i :

$$\psi(\vec{\sigma}) = \cosh(W_1\sigma_1 + W_2\sigma_2 + \dots + W_L\sigma_L). \quad (38)$$

A more intuitive way to think about this is that the network needs to maximize the distance between $\psi(\uparrow\uparrow \dots \uparrow)$ and all other wave function coefficients, which can only be achieved in the large W_i limit.

Locally analytic NQS.— Next, we comment on NQS with activation functions that are only locally analytic. These functions have a finite convergence radius and, thus, do not necessarily have the same polynomial behavior for all basis states. However, this can simplify the optimization. Locally analytic functions have at least two regimes with distinct behavior. This allows to separate or group basis states by shifting them in different regimes. A prominent example for locally analytic functions is the

rectified linear unit (ReLU):

$$\text{ReLU}(x) = \begin{cases} x & \text{for } x > 0, \\ 0 & \text{for } x \leq 0. \end{cases} \quad (39)$$

As can be readily seen, the ReLU will not increase the order of correlations in the system; nonetheless, it is a very efficient activation function. Instead of building up correlations, it has the ability to group states by tuning the bias, which allows to set probabilities of multiple basis states to zero. The system can then use all the other network parameters to represent the wave function coefficients of the remaining states. An example for a transverse field Ising model ($\hat{H}_{\text{TFIM}} = \hat{H}_{\text{Ising}} - h_x \sum_i \hat{\sigma}_i^x$) on a $L \times L = 4 \times 4$ lattice is shown in Fig. 4b). Here, the feed forward neural network achieves good results by tuning the bias such that the ReLU activation sets the wave function coefficients of most basis states to zero. Specifically, the wave function has nonzero coefficients for only 17 basis states (out of $\mathcal{O}(10^5)$). This is not a coincidence, since the NQS has access to precisely 17 correlations (one bias ($\mathcal{X}_0 = 0^{\text{th}}$ order) and $L \times L = 16$ first order correlations, compare with Eq. (16)). In the context of a system of equations, introduced in Sec. VI, this implies that, when learning the perturbed AFM state, the network can faithfully solve the set of equations for at most 17 basis states. Similarly, other locally analytic functions like tanh or sigmoid have the ability to group basis states, such that the optimization can potentially be simplified.

X. COMMENT ON NETWORK ARCHITECTURES

In the following, we want to use the acquired knowledge about the working principle of NQS and their representational power to comment on potential advantages

and disadvantages of commonly used network architectures.

Autoregressive NQS.— In the research of neural quantum states, two directions have emerged, namely non-autoregressive methods based on Metropolis Hastings Monte Carlo, where the machine learning model outputs the full wave function at once, and autoregressive NQS that evaluate the amplitude of the full wave function as a product of local, conditional probabilities:

$$p(\vec{\sigma}) = p(\sigma_1)p(\sigma_2|\sigma_{\leq 1})\dots p(\sigma_L|\sigma_{\leq L-1}). \quad (40)$$

Thus, the machine learning model gradually acquires information about the input and has to adjust its conditional probabilities accordingly. Each conditional probability $p(\sigma_k|\sigma_{\leq k-1})$ can be written in its orthogonal correlator basis according to Eq. (12):

$$p(\sigma_k|\sigma_{\leq k-1}) = \sum_{S \subseteq [k]} \bar{p}_k(S) \mathcal{X}_S(\sigma), \quad (41)$$

where $\bar{p}_k(S)$ is defined as:

$$\bar{p}_k(S) = \frac{1}{2^k} \sum_{\vec{\sigma} \in \{-1,1\}^k} p(\sigma_k|\sigma_{\leq k-1}) \mathcal{X}_S(\sigma). \quad (42)$$

Therefore, the total probability $p(\vec{\sigma})$ is by design a construction that contains all correlation functions, which is required for a good approximation of many quantum states. Thus, the relevant criterion for autoregressive NQS is the difficulty to represent the conditional probabilities $p(\sigma_k|\sigma_{\leq k-1})$, which has a complexity of $\mathcal{O}(2^k)$ (in total $\mathcal{O}(2^{\sum_{k=1}^L k})$). However, many quantum state satisfy conditional independence:

$$p(\sigma_k|\sigma_{k-1 \geq}) = p(\sigma_k|\sigma_{k-1}, \sigma_{k-2}, \dots, \sigma_{k-l}), \quad (43)$$

with small l , which reduces the complexity of the full problem to approximately $\mathcal{O}(L \times 2^l)$, such that an efficient representation can be found [38]. The term short ranged conditional probabilities can be translated to our formalism in Eq. (42), as it is equivalent to setting the correlation order coefficient $\bar{p}_k(S)$ to zero, if S contains any σ_j with $j \leq k-l-1$.

Note that autoregressive models have an inherent non-symmetric feature in the architecture due to their path-like structure (see Eq. (40)) [13], as the first site only depends on itself, while the probability on the last site depends on all sites. This will also become obvious when writing Eq. (40) in terms of $\bar{p}_k(S)$ and $\mathcal{X}_S(\sigma)$. The more short ranged a conditional probability is (compare with Eq. (43)), the more symmetric the equation becomes.

Non-autoregressive NQS.— Non-autoregressive NQS model the full wave function directly, without factorizing it into a sequence of conditional probabilities. Therefore, this requires network architectures to be capable of generating high correlations orders. This is reflected in the development of the current research direction. Early approaches often relied on Restricted Boltzmann machines,

due to their analytical accessibility [16, 20]. However, the lack of complexity results in an inefficient way to generate large coefficients for high correlation orders. This limitation has unwittingly led to the adoption of architectures that can naturally generate high correlation orders with large coefficients.

Transformer neural quantum states are a prominent example [8, 22, 51–53]: the multiplicative terms in the attention mechanism naturally produce large coefficients for higher correlation orders:

$$\text{Attention}(Q, K, V) = \text{softmax}\left(\frac{QK^T}{\sqrt{d_k}}\right)V, \quad (44)$$

where Q, K, V are all linear in the input, which itself can be a sum over multiple correlation orders.

Similarly, determinant-based architectures have become the unchallenged architecture for fermionic [7, 54, 55] systems. To illustrate that determinant wave functions generate large coefficients for high correlation orders efficiently, we discuss neural backflow based determinant constructions for m fermions on L sites [2, 37]:

$$\Psi(\vec{n}) = \det \begin{vmatrix} \phi_{k_1 1}^{\text{bf}}(n_1, \dots, n_L) & \dots & \phi_{k_1 m}^{\text{bf}}(n_1, \dots, n_L) \\ \vdots & \ddots & \vdots \\ \phi_{k_m 1}^{\text{bf}}(n_1, \dots, n_L) & \dots & \phi_{k_m m}^{\text{bf}}(n_1, \dots, n_L) \end{vmatrix}, \quad (45)$$

where $\phi_{k_i j}^{\text{bf}}(n_1, \dots, n_n)$ are backflow enhanced elements. k_i denotes the index of the i^{th} occupied site and j represents the j^{th} fermion. In a backflow based determinant, one introduces the potentially deep neural network $f_{k_i j}^{\theta}(n_1, \dots, n_n)$ that uses Fock space configurations as inputs, at an orbital level:

$$\phi_{k_i j}^{\text{bf}}(n_1, \dots, n_n) = \phi_{k_i j} + f_{k_i j}^{\theta}(n_1, \dots, n_n). \quad (46)$$

Therefore, $\phi_{k_i j}^{\text{bf}}(n_1, \dots, n_n)$ itself, can be a function with higher-order correlations. Importantly, however, the determinant structure acts as a further non-linear activation function: by involving products of system size many orbital, it automatically generates large coefficients for higher-order correlations:

$$\Psi(\vec{n}) = \sum_{i_1, \dots, i_m} \epsilon_{i_1, \dots, i_m} \phi_{k_1, i_1}^{\text{bf}} \dots \phi_{k_m, i_m}^{\text{bf}}. \quad (47)$$

A natural consequence can be that the specific choice of neural network architecture is less critical [56].

Since both network architectures are designed to naturally generate large coefficients for high correlation orders, they appear— from the correlator’s perspective— to be highly suitable for NQS simulations. This has been confirmed in numerous numerical benchmarks, where they outperformed other architectures [14, 33, 57–59].

XI. CONCLUSION

In this work, we explored the importance of correlations in neural quantum states (NQS), in particular, how

they determine a network’s ability to faithfully represent quantum states. By using correlation based neural networks, we were able to numerically demonstrate that even simple quantum states, such as product states, can require all possible correlation orders for an accurate representation, whereas other, more complex quantum states can be represented using a simple correlation structure in a restricted Hilbert space.

Using tools from Boolean function theory, we provided a framework to better understand the requirements for NQS-like quantum state representation. This framework reveals that the internal NQS structure effectively represents a quantum state in the correlator basis and, consequently, requires a basis transformation from the computational basis, which can lead to non-trivial correlation order structures.

Furthermore, we employed this formalism to understand the consequences of Hilbert space truncation, which introduces linear dependencies in the correlator basis and therefore results, in most cases, in multiple possible solutions for the quantum state representation. Additionally, we showed connections between spin basis rotations and the correlator basis, which can provide valuable insights about the desired NQS structure and potential problems for quantum state representation.

Finally, we investigated how activation functions and neural network architectures influence the expressiveness of the neural quantum state ansatz. These design choices affect the ability to group certain basis states or to generate large coefficients for high-order terms, which strongly influences the correlations that can be captured and, consequently, the network’s representational power.

Overall, our results offer new insights into the internal structure of NQS and allow a deeper understanding of its requirements. By identifying the key role of correlations in neural quantum states and clarifying how these correlations emerge from the network architecture, we provide a foundation for a systematic tailoring and optimization of NQS to a desired quantum system.

Note added.— While finishing the manuscript, we became aware of a related work by Schurov et al. [50], studying the complexity of sign structures using Boolean Fourier analysis.

of Bavaria under the Excellence Strategy of the Federal Government and the Länder and by the Deutsche Forschungsgemeinschaft (DFG, German Research Foundation) under Germany’s Excellence Strategy (EXC-2111 – 390814868).

CODE AND DATA AVAILABILITY

Code and data are available from the corresponding author on request.

ACKNOWLEDGMENTS

We thank F. Pauw, T. Vovk, C. Roth, and D. Aliverti-Piuri for fruitful discussions. This research was supported by LMUexcellent, funded by the Federal Ministry of Education and Research (BMBF) and the Free State

Appendix A: Correlator Transformer: Detailed Description

A major disadvantage of neural quantum states (NQS) is the limited understanding of their optimization and representation processes. Although we have techniques that minimize the energy or evolve the state in time (and so on), we have no intuition why certain parameters might be relevant or irrelevant.

To investigate this behavior, we employ a correlator transformer as an architecture for neural quantum states. The correlator transformer was introduced in Suresh et al. [42]. The model uses standard patched input configurations $\sigma_{i,p}$ with a linear embedding:

$$X_{i,m}^1 = \sum_p \sigma_{i,p} W_{p,m} \text{pE}_{i,m}, \quad X^1 \in \mathbb{R}^{(L_x/p, L_y/p, 2p)}, \quad (\text{A1})$$

where i indexes the patch, p labels the position within a patch, and m denotes the embedding dimension. Here, $W_{p,m}$ are trainable network parameters and $\text{pE}_{i,m}$ represents the standard positional encoding:

$$\text{pE}_{i,m} = \begin{cases} \sin\left(\frac{i}{10000^{2j/d}}\right) & m = 2j, \\ \cos\left(\frac{i}{10000^{2j/d}}\right) & m = 2j + 1. \end{cases} \quad (\text{A2})$$

The matrix $X_{i,m}^1$ that contains first order correlations is then used to calculate the query Q_n and key K_n values of the transformer:

$$Q_n = X^1 W^{nQ} \quad \text{and} \quad K_n = X^n W^{nK}, \quad (\text{A3})$$

the value matrix, on the other hand, is given by: $V_n = \text{pE} W^{nV}$ where W^{nQ} , W^{nK} and W^{nV} are network weights. A product of query, key, and value matrices defines the output of the corresponding layer:

$$X^{n+1} = \frac{1}{\sqrt{2p}} Q_n K_n^T V_n. \quad (\text{A4})$$

All outputs $\mathbb{X} = [\bar{X}^1, \bar{X}^2, \dots, \bar{X}^i, \dots, \bar{X}^n]$, with $\bar{X}^i = \text{mean}(X^i)$ are then used in a linear layer, with weights W^{pred} , to predict the probability of the corresponding input configuration:

$$\psi(\vec{\sigma}) = W^{\text{pred}} \mathbb{X}(\vec{\sigma}) + \beta. \quad (\text{A5})$$

This wave function of polynomial form allows us to interpret the processes within the transformer. Here, we included the bias β as this corresponds to 0th order correlations.

Number of parameters.— To ensure a fair comparison between different correlation orders, we keep the total number of trainable parameters approximately constant. The total number of parameters depends on the system size ($N_x \times N_y$), the patch size p_{size} , and the embedding dimension e_{dim} .

The equation that defines the number of parameters is given by:

$$\begin{aligned} \# \text{params} = & \underbrace{(p_{\text{size}} e_{\text{dim}})}_{\text{embedding}} + \underbrace{\frac{N_x N_y}{p_{\text{size}}} e_{\text{dim}}}_{\text{pE}} \\ & + \underbrace{3(n_{\text{lay}} - 1) e_{\text{dim}}^2}_{\text{decoder}} + \underbrace{n_{\text{lay}} + 1}_{W^{\text{pred}} + \beta} \end{aligned} \quad (\text{A6})$$

Appendix B: Generalizing to other encodings and non-spin systems

In the main text we focused our analysis on spin-1/2 systems. However, the idea to expand systems in terms of monomials of the input can be extended to systems with one-hot encoding or to cases with higher local Hilbert space dimensions.

One-hot encoding.— We start by discussing one-hot encoding for general systems. This method embeds the Hilbert space of the system in a much larger one and truncates it afterward. To provide an intuitive example, we stick to a system with $\{-1, 1\}^L$ spins. When using one-hot encoding, the effective Hilbert space is given by: $\{\{0, 1\}, \{0, 1\}\}^L$. Since we are not interested in the whole effective Hilbert space, we truncate it and use the decision tree formalism. The indicator polynomial of the extended local Hilbert space is given by:

$$\begin{aligned} \mathbb{1}_{\alpha, \beta}(\sigma^s) &= \mathbb{1}_{\alpha}(\sigma_1^s) \mathbb{1}_{\beta}(\sigma_2^s) = \\ &= \sum_{\alpha, \beta \in \{0, 1\}^L} \frac{1 - 4(\alpha - \frac{1}{2})(\sigma_1^s - \frac{1}{2})}{2} \frac{1 - 4(\beta - \frac{1}{2})(\sigma_2^s - \frac{1}{2})}{2}, \end{aligned} \quad (\text{B1})$$

which reduces to:

$$\mathbb{1}_{\alpha/\beta}(\sigma_{1/2}^s) = \begin{cases} \sigma_{1/2}^s & \text{for } \alpha/\beta = 1, \\ 1 - \sigma_{1/2}^s & \text{for } \alpha/\beta = 0. \end{cases} \quad (\text{B2})$$

This produces a polynomial similar to Eq. 12 (considering that $\sigma_1^s = 1 - \sigma_2^s$). Hence, one hot encoding does not offer an immediate advantage (or disadvantage) compared to typical spin encoding. Note that the monomials are no longer orthogonal. Nevertheless, this expression can be useful, as it allows a relatively simple understanding of how it groups states: Terms of degree k contribute to the coefficient of 2^{L-k} basis states. Therefore, characterizing a basis state requires one system size order correlation. E.g. a product state of up spins is given by $\psi_{\uparrow}(\vec{\sigma}) = \prod_{i=1}^L \sigma_{2,i}$, whereas down spins are given by $\psi_{\downarrow}(\vec{\sigma}) = \prod_{i=1}^L \sigma_{1,i}$.

Non binary local Hilbert space dimension.— Finally, we turn to systems with larger local Hilbert spaces and non binary encoding. To do so, we introduce the Lagrange basis, a more general form of the indicator

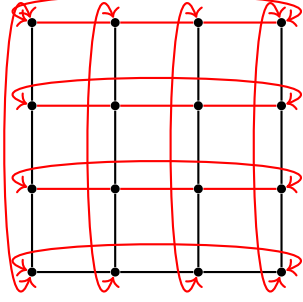


FIG. 5. Spanning tree (black links) for a toric code model restricted to the physical sector. The $N_x \times N_y + 1$ spins on the red links span the full orthogonal basis, spins on black links are determined by the configuration of the red links due to Gauss's law.

polynomial [60–62]. It defines an orthonormal basis $\{l_1(x^s), l_2(x^s), \dots, l_k(x^s)\}$ at site s for a local Hilbert space dimension $\{x_1^s, x_2^s, \dots, x_k^s\}$ of k . The polynomial $l_{\alpha^s}(x^s)$ is defined by:

$$l_{\alpha_j^s}(x^s) = \prod_{\substack{0 \leq m \leq k \\ m \neq j}} \frac{x^s - \alpha_m^s}{\alpha_j^s - \alpha_m^s} = \begin{cases} 1 & \text{for } x^s = \alpha_j^s, \\ 0 & \text{else.} \end{cases} \quad (\text{B3})$$

with $x^s, \alpha_j^s \in \{x_1^s, x_2^s, \dots, x_k^s\}$. The complete orthonormal basis for all sites S is then defined by:

$$L_{\vec{\alpha}}(\vec{x}) = \prod_{s \in S} l_{\alpha^s}(x^s), \quad (\text{B4})$$

which allows to write the wave function as:

$$\psi(\vec{x}) = \sum_{\vec{\alpha} \in \{x_1, \dots, x_k\}^n} \psi(\vec{\alpha}) L_{\vec{\alpha}}(\vec{x}). \quad (\text{B5})$$

Thus, the resulting wave function is a polynomial of degree $(k-1) \times n$. Although the analysis in this regime becomes more challenging, as the maximal polynomial order grows much faster with system size and its monomials are no longer orthogonal, we can still conclude that even for simple product states high expansion orders are required.

Appendix C: Spanning tree formalism applied to the toric code model restricted to the physical sector

Studying the perturbed toric code model is a difficult task as the Hilbert space grows with $2^{2(L_x \times L_y)}$. However, restricting the analysis to the physical sector, where Gauss's law is always fulfilled, reduces the effective Hilbert space dimension to $2^{L_x \times L_y + 1}$. Following the

spanning tree formalism allows to limit the number of relevant spins to $L_x \times L_y + 1$ [45, 63, 64]. This is shown in Fig. 5. Spins on the black links determine the full configuration and span the complete orthogonal basis (according to Eq. (14)). Consequently, the remaining $L_x \times L_y - 1$ spins on the red links are linearly dependent on the “basis spins” and thus contain relevant information about potentially higher-order correlations of the $L_x \times L_y + 1$ basis spins.

Note that the spanning tree shown in Fig. 5 is not unique: translations and rotations of this tree will yield an equally well-suited orthogonal basis.

-
- [1] W. M. C. Foulkes, L. Mitas, R. J. Needs, and G. Rajagopal, “Quantum monte carlo simulations of solids,” *Rev. Mod. Phys.* **73**, 33–83 (2001).
- [2] Federico Becca and Sandro Sorella, *Quantum Monte Carlo Approaches for Correlated Systems* (Cambridge University Press, 2017).
- [3] Gaopei Pan and Zi Yang Meng, “The sign problem in quantum monte carlo simulations,” in *Encyclopedia of Condensed Matter Physics* (Elsevier, 2024) p. 879–893.
- [4] Ulrich Schollwöck, “The density-matrix renormalization group in the age of matrix product states,” *Annals of Physics* **326**, 96–192 (2011).
- [5] Giuseppe Carleo and Matthias Troyer, “Solving the quantum many-body problem with artificial neural networks,” *Science* **355**, 602–606 (2017).
- [6] Ao Chen and Markus Heyl, “Empowering deep neural quantum states through efficient optimization,” *Nature Physics* **20**, 1476–1481 (2024).
- [7] Ao Chen, Zhou-Quan Wan, Anirvan Sengupta, Antoine Georges, and Christopher Roth, “Neural Network-Augmented Pfaffian Wave-functions for Scalable Simulations of Interacting Fermions,” (2025), [arXiv:2507.10705 \[cond-mat.str-el\]](#).
- [8] Luciano Loris Viteritti, Riccardo Rende, and Federico Becca, “Transformer variational wave functions for frustrated quantum spin systems,” *Phys. Rev. Lett.* **130**, 236401 (2023).
- [9] Hannah Lange, Anka Van de Walle, Atiye Abedinnia, and Annabelle Bohrdt, “From architectures to applications: a review of neural quantum states,” *Quantum Science and Technology* **9**, 040501 (2024).
- [10] Markus Schmitt and Markus Heyl, “Simulating dynamics of correlated matter with neural quantum states,” (2025), [arXiv:2506.03124 \[quant-ph\]](#).
- [11] Clemens Giuliani, Filippo Vicentini, Riccardo Rossi, and Giuseppe Carleo, “Learning ground states of gapped quantum Hamiltonians with Kernel Methods,” *Quantum* **7**, 1096 (2023).
- [12] Hannah Lange, Fabian Döschl, Juan Carrasquilla, and Annabelle Bohrdt, “Neural network approach to quasiparticle dispersions in doped antiferromagnets,” *Communications Physics* **7**, 187 (2024).
- [13] Fabian Döschl, Felix A. Palm, Hannah Lange, Fabian Grusdt, and Annabelle Bohrdt, “Neural network quantum states for the interacting hofstadter model with higher local occupations and long-range interactions,” *Phys. Rev. B* **111**, 045408 (2025).
- [14] Zakari Denis, Alessandro Sinibaldi, and Giuseppe Carleo, “Comment on “can neural quantum states learn volume-law ground states?”,” *Phys. Rev. Lett.* **134**, 079701 (2025).
- [15] Dominik S. Kufel, Jack Kemp, DinhDuy Vu, Simon M. Linsel, Chris R. Laumann, and Norman Y. Yao, “Approximately symmetric neural networks for quantum spin liquids,” *Phys. Rev. Lett.* **135**, 056702 (2025).
- [16] Xun Gao and Lu-Ming Duan, “Efficient representation of quantum many-body states with deep neural networks,” *Nature Communications* **8**, 662 (2017).
- [17] Or Sharir, Amnon Shashua, and Giuseppe Carleo, “Neural tensor contractions and the expressive power of deep neural quantum states,” *Phys. Rev. B* **106**, 205136 (2022).
- [18] Dong-Ling Deng, Xiaopeng Li, and S. Das Sarma, “Quantum entanglement in neural network states,” *Phys. Rev. X* **7**, 021021 (2017).
- [19] Ivan Glasser, Nicola Pancotti, Moritz August, Ivan D. Rodriguez, and J. Ignacio Cirac, “Neural-network quantum states, string-bond states, and chiral topological states,” *Phys. Rev. X* **8**, 011006 (2018).
- [20] Giuseppe Carleo, Yusuke Nomura, and Masatoshi Imada, “Constructing exact representations of quantum many-body systems with deep neural networks,” *Nature Communications* **9** (2018).
- [21] Harel Kol-Namer and Moshe Goldstein, “Neural network ground state from the neural tangent kernel perspective: The sign bias,” (2024), [arXiv:2411.03980 \[quant-ph\]](#).
- [22] Riccardo Rende, Luciano Loris Viteritti, Lorenzo Bardone, Federico Becca, and Sebastian Goldt, “A simple linear algebra identity to optimize large-scale neural network quantum states,” *Communications Physics* **7**, 260 (2024).
- [23] Sidhartha Dash, Luca Gravina, Filippo Vicentini, Michel Ferrero, and Antoine Georges, “Efficiency of neural quantum states in light of the quantum geometric tensor,” *Communications Physics* **8** (2025).
- [24] M. Schuyler Moss, Alev Orfi, Christopher Roth, Anirvan M. Sengupta, Antoine Georges, Dries Sels, Anna Dawid, and Agnes Valenti, “Double descent: When do neural quantum states generalize?” (2025), [arXiv:2508.00068 \[cond-mat.dis-nn\]](#).
- [25] Giacomo Passetti, Damian Hofmann, Pit Neitemeier, Lukas Grunwald, Michael A. Sentef, and Dante M. Kennes, “Can neural quantum states learn volume-law ground states?” *Phys. Rev. Lett.* **131**, 036502 (2023).
- [26] G. Cybenko, “Approximation by superpositions of a sigmoidal function,” *Mathematics of Control, Signals and Systems* **2**, 303–314 (1989).
- [27] Kurt Hornik, Maxwell Stinchcombe, and Halbert White, “Multilayer feedforward networks are universal approximators,” *Neural Networks* **2**, 359–366 (1989).
- [28] Kurt Hornik, Maxwell Stinchcombe, and Halbert White, “Universal approximation of an unknown mapping and its derivatives using multilayer feedforward networks,” *Neural Networks* **3**, 551–560 (1990).
- [29] Mohamed Hibat-Allah, Roger G. Melko, and Juan Carrasquilla, “Investigating topological order using recurrent neural networks,” *Phys. Rev. B* **108**, 075152 (2023).
- [30] Mohamed Hibat-Allah, Estelle M. Inack, Roeland Wiersema, Roger G. Melko, and Juan Carrasquilla, “Variational neural annealing,” *Nature Machine Intelligence* **3**, 952–961 (2021).
- [31] David Pfau, Simon Axelrod, Halvard Sutterud, Ingrid von Glehn, and James S. Spencer, “Accurate computation of quantum excited states with neural networks,” *Science* **385** (2024).
- [32] Yuntian Gu, Wenrui Li, Heng Lin, Bo Zhan, Ruichen Li, Yifei Huang, Di He, Yantao Wu, Tao Xiang, Mingpu Qin, Liwei Wang, and Dingshun Lv, “Solving the hubbard model with neural quantum states,” (2025), [arXiv:2507.02644 \[cond-mat.str-el\]](#).
- [33] Ao Chen, Vighnesh Dattatraya Naik, and Markus Heyl, “Convolutional transformer wave functions,” (2025),

- arXiv:2503.10462 [cond-mat.dis-nn].
- [34] Zakari Denis and Giuseppe Carleo, “Accurate neural quantum states for interacting lattice bosons,” *Quantum* **9**, 1772 (2025).
 - [35] Dong-Ling Deng, Xiaopeng Li, and S. Das Sarma, “Machine learning topological states,” *Phys. Rev. B* **96**, 195145 (2017).
 - [36] Raphael Kaubruegger, Lorenzo Pastori, and Jan Carl Budich, “Chiral topological phases from artificial neural networks,” *Phys. Rev. B* **97**, 195136 (2018).
 - [37] Sirui Lu, Xun Gao, and L.-M. Duan, “Efficient representation of topologically ordered states with restricted boltzmann machines,” *Phys. Rev. B* **99**, 155136 (2019).
 - [38] Tai-Hsuan Yang, Mehdi Soleimanifar, Thiago Bergamaschi, and John Preskill, “When can classical neural networks represent quantum states?” (2024), arXiv:2410.23152 [quant-ph].
 - [39] Agnes Valenti, Eliska Greplova, Netanel H. Lindner, and Sebastian D. Huber, “Correlation-enhanced neural networks as interpretable variational quantum states,” *Phys. Rev. Res.* **4**, L012010 (2022).
 - [40] “Correlator convolutional neural networks as an interpretable architecture for image-like quantum matter data,” *Nature Communications* **12**, 3905 (2021).
 - [41] Kirsten Fischer, Alexandre René, Christian Keup, Moritz Layer, David Dahmen, and Moritz Helias, “Decomposing neural networks as mappings of correlation functions,” *Phys. Rev. Res.* **4**, 043143 (2022).
 - [42] Abhinav Suresh, Henning Schlömer, Baran Hashemi, and Annabelle Bohrdt, “Interpretable correlator transformer for image-like quantum matter data,” *Machine Learning: Science and Technology* **6**, 025006 (2025).
 - [43] Kacper Cybiński, James Enouen, Antoine Georges, and Anna Dawid, “Speak so a physicist can understand you! tetriscnn for detecting phase transitions and order parameters,” (2024), arXiv:2411.02237 [quant-ph].
 - [44] Di Luo, Giuseppe Carleo, Bryan K. Clark, and James Stokes, “Gauge equivariant neural networks for quantum lattice gauge theories,” *Physical Review Letters* **127** (2021).
 - [45] Yarden Sheffer, Erez Berg, and Ady Stern, “Preparing topological states with finite depth simultaneous commuting gates,” *Phys. Rev. B* **111**, 115160 (2025).
 - [46] Ryan O’Donnell, *Analysis of Boolean Functions* (Cambridge University Press, 2014).
 - [47] Mohamed Hibat-Allah, Martin Ganahl, Lauren E. Hayward, Roger G. Melko, and Juan Carrasquilla, “Recurrent neural network wave functions,” *Phys. Rev. Res.* **2**, 023358 (2020).
 - [48] Mohamed Hibat-Allah, Roger G. Melko, and Juan Carrasquilla, “Supplementing recurrent neural network wave functions with symmetry and annealing to improve accuracy,” (2024), arXiv:2207.14314 [cond-mat.dis-nn].
 - [49] Marin Bukov, Markus Schmitt, and Maxime Dupont, “Learning the ground state of a non-stoquastic quantum Hamiltonian in a rugged neural network landscape,” *SciPost Phys.* **10**, 147 (2021).
 - [50] Ilya Schurov, Anna Kravchenko, Mikhail I. Katsnelson, Andrey A. Bagrov, and Tom Westerhout, “Learning complexity of many-body quantum sign structures through the lens of boolean fourier analysis,” (2025), arXiv:2508.09870 [cond-mat.dis-nn].
 - [51] Yangjun Wu, Chu Guo, Yi Fan, Pengyu Zhou, and Honghui Shang, “Nnqs-transformer: an efficient and scalable neural network quantum states approach for ab initio quantum chemistry,” in *Proceedings of the International Conference for High Performance Computing, Networking, Storage and Analysis* (Association for Computing Machinery, New York, NY, USA, 2023).
 - [52] Luciano Loris Viteritti, Riccardo Rende, Alberto Parola, Sebastian Goldt, and Federico Becca, “Transformer wave function for two dimensional frustrated magnets: Emergence of a spin-liquid phase in the shastry-sutherland model,” *Physical Review B* **111** (2025), 10.1103/physrevb.111.134411.
 - [53] Hannah Lange, Guillaume Bornet, Gabriel Emperauger, Cheng Chen, Thierry Lahaye, Stefan Kienle, Antoine Browaeys, and Annabelle Bohrdt, “Transformer neural networks and quantum simulators: a hybrid approach for simulating strongly correlated systems,” *Quantum* **9**, 1675 (2025).
 - [54] Javier Robledo Moreno, Giuseppe Carleo, Antoine Georges, and James Stokes, “Fermionic wave functions from neural-network constrained hidden states,” *Proceedings of the National Academy of Sciences* **119**, e2122059119 (2022).
 - [55] Björn J. Wurst, Dante M. Kennes, and Jonas B. Profe, “Efficiency of the hidden fermion determinant states ansatz in the light of different complexity measures,” *Phys. Rev. Res.* **7**, 023316 (2025).
 - [56] Hannah Lange, Annika Böhrer, Christopher Roth, and Annabelle Bohrdt, “Simulating the two-dimensional $t-j$ model at finite doping with neural quantum states,” (2024), arXiv:2411.10430 [cond-mat.str-el].
 - [57] Di Luo and Bryan K. Clark, “Backflow transformations via neural networks for quantum many-body wave functions,” *Physical Review Letters* **122** (2019).
 - [58] Riccardo Rende, Sebastian Goldt, Federico Becca, and Luciano Loris Viteritti, “Fine-tuning neural network quantum states,” *Phys. Rev. Res.* **6**, 043280 (2024).
 - [59] Kenny Choo, Antonio Mezzacapo, and Giuseppe Carleo, “Fermionic neural-network states for ab-initio electronic structure,” *Nature Communications* **11**, 2368 (2020).
 - [60] Edward Waring, “Vii. problems concerning interpolations,” *Philosophical Transactions of the Royal Society of London* **69**, 59–67 (1779).
 - [61] Alexandre M. Bayen and Timmy Siau, “Chapter 14 - interpolation,” in *An Introduction to MATLAB® Programming and Numerical Methods for Engineers*, edited by Alexandre M. Bayen and Timmy Siau (Academic Press, Boston, 2015) pp. 211–223.
 - [62] Michael Lindsey, “Multiscale interpolative construction of quantized tensor trains,” (2024), arXiv:2311.12554 [math.NA].
 - [63] Nicolai Lang and Hans Peter Büchler, “Minimal instances for toric code ground states,” *Phys. Rev. A* **86**, 022336 (2012).
 - [64] Wuxu Zhao, Menglong Fang, and Daiqin Su, “A graph-based approach to entanglement entropy of quantum error correcting codes,” (2025), arXiv:2501.06407 [quant-ph].